A LETTERS JOURNAL EXPLORING THE FRONTIERS OF PHYSICS

OFFPRINT

Critical jamming of frictional grains in the generalized isostaticity picture

S. HENKES, M. VAN HECKE and W. VAN SAARLOOS

EPL, **90** (2010) 14003

A Letters Journal Exploring the Frontiers of Physics

April 2010

EPL, **90** (2010) 14003
doi: 10.1209/0295-5075/90/14003

www.epljournal.org

Critical jamming of frictional grains in the generalized isostaticity picture

S. Henkes[1(a)], M. van Hecke[2] and W. van Saarloos[2]

[1] *Instituut-Lorentz, LION, Leiden University - P.O. Box 9506, 2300 RA Leiden, The Netherlands*
[2] *Kamerlingh Onnes Laboratory, LION, Leiden University - P.O. Box 9504, 2300 RA Leiden, The Netherlands*

received 30 September 2009; accepted in final form 24 March 2010
published online 4 May 2010

PACS 45.70.-n – Granular systems
PACS 46.55.+d – Tribology and mechanical contacts
PACS 63.50.-x – Vibrational states in disordered systems

Abstract – While frictionless spheres at jamming are isostatic, frictional spheres at jamming are not. As a result, frictional spheres near jamming do not necessarily exhibit an excess of soft modes. However, a generalized form of isostaticity can be introduced if fully mobilized contacts at the Coulomb friction threshold are considered as slipping contacts. We show here that, in this framework, the vibrational density of states (DOS) of frictional discs exhibits a plateau when the generalized isostaticity line is approached. The crossover frequency ω^* scales linearly with the distance from this line. Moreover, we show that the frictionless limit, which appears singular when fully mobilized contacts are treated elastically, becomes smooth when fully mobilized contacts are allowed to slip. Finally, we elucidate the nature of the vibrational modes, both for slipping and for non-slipping fully mobilized contacts.

The jamming transition in disordered media has been the focus of intensive research efforts in recent years. Most work has focussed on the simplest case of purely repulsive frictionless spheres that jam when the pressure becomes positive. The corresponding jamming point, known as point J, acts as a critical point: close to it one observes non-trivial powerlaw scaling of the elastic constants, an abundance of soft modes, a diverging length-scale and singularly non-affine behavior [1–4]. These phenomena are deeply rooted in the emergence of isostaticity at the jamming point: for frictionless spheres, the packings reached for vanishingly small pressure are marginally stable and the contact number z at point J reaches $z^0_{\rm iso} = 2d$, where d is the number of spatial dimensions [1].

What is becoming clear for the last two years is that isostaticity and jamming do not go hand in hand for soft particles with different interactions [5–8]. In particular, friction has to be introduced to make connection with the granular systems studied in experiments [9], in engineering [10] and in the geosciences [11]. For frictional spheres, the contact number at the jamming transition, z_c, lies between the frictional isostatic value $z^\mu_{\rm iso} = d+1$ and the frictionless isostatic value $z^0_{\rm iso} = 2d$, depending on the preparation method and the friction coefficient μ of the material. Hence, isostaticity and jamming do not coincide for frictional spheres, and the central question is to understand how friction modifies the critical jamming scenario developed for frictionless spheres.

The density of states (DOS) has played a crucial role in understanding the jamming scenario, and for *frictionless* spheres the spectrum of vibrational modes shows an excess density of states at low frequencies, with a finite number of zero-energy modes at the jamming transition and a cross-over frequency $\omega^* \sim (z - z^0_{\rm iso})$ [2,3]. Calculating the DOS for *frictional* discs, Somfai *et al.* studied the cross-over frequency ω^* in the presence of friction and concluded that ω^* scales with the distance to the frictional isostatic limit $(z - z^\mu_{\rm iso})$, but *not* with distance to the frictional jamming transition $(z - z_c)$: $\omega^* \sim (z - z^\mu_{\rm iso})$ [6].

We will show here that so-called fully mobilized contacts, contacts where the tangential force reaches the maximum allowed by the Coulomb criterium, play a crucial role for jamming of frictional spheres. In the work of Somfai *et al.* [6], all contacts where assumed to be non-sliding under small vibrations. Since it is far from obvious how fully mobilized contacts react to tangential perturbations, the question is raised how to deal with vibrations in the presence of such contacts. Here we

(a) E-mail: henkes@lorentz.leidenuniv.nl

will show that when fully mobilized contacts are seen as sliding, dramatically different densities of states are obtained —in particular, the crossover frequency ω^* then scales with distance to the pertinent generalized isostatic number, $z = z^m_{\rm iso}$.

To make the notion of generalized isostaticity concrete, note that the frictional isostatic value $z^\mu_{\rm iso}$ derives from a counting argument assuming *arbitrary* tangential friction forces, and is reached in practice at jamming in the limit $\mu \to \infty$, for gently prepared packings [5,12,13]. However, the magnitude of the tangential forces is limited by the Coulomb criterion $|f_t| \leqslant \mu f_n$. Let $m = |f_t|/\mu f_n$ be the mobilization of a contact, such that contacts at the Coulomb threshold, so-called fully mobilized contacts, have $m = 1$. The crucial finding of [5] is that due to sliding, a *finite* fraction of contacts can be fully mobilized. Contacts which reach the mobilization threshold slip with unchanged tangential forces if the perturbation in the direction of mobilization continues. This leads to a well-defined δ-peak in the integrated mobilization distribution, as shown in fig. 2b of [5]. This result affects the counting arguments, and suggests to generalize the isostaticity condition [5,14,15].

To derive the generalized isostaticity condition, we define $n_m \in [0, z/2]$ as the fraction of contacts per particle at the Coulomb threshold, where the factor of 2 is due to each contact being shared by 2 particles. For frictional particles, the tangential forces introduce $d-1$ additional force components at each contact. Then for a packing to be stable, the $Nd(d+1)/2$ rotational and translational degrees of freedom need to be constrained by the $Nzd/2 - Nn_m$ independent force components. This lead Shundyak *et al.* [5] to propose the *generalized isostaticity* criterion

$$z \geqslant (d+1) + \frac{2n_m}{d} \equiv z^m_{\rm iso}. \qquad (1)$$

This inequality implies that there is a range of contact numbers larger than the ordinary isostaticity criterion, but smaller than the generalized isostaticity criterion. Which criterion is relevant? Simulations have shown that as frictional packings are prepared gently, the fraction of fully mobilized contacts at jamming is such that z approaches the generalized isostaticity line $z = z^m_{\rm iso}$ in the (z, n_m)-plane (fig. 1), in accord with an earlier suggestion by Bouchaud [15]. Hence, generalized isostaticity gives a more complete prediction of frictional packings near jamming.

The exact values of n_m for $0 < \mu < \infty$ depend on the preparation method [13,16], but in the limit of very "gentle" equilibration so as to approach the jamming threshold, they are a smooth decreasing function of μ [5,12,13,17,18]. For $2d$ systems in particular, one finds that $n_m \to 1$ in the frictionless limit since $z \approx z^0_{\rm iso} = 4$, while $n_m \to 0$ in the limit $\mu \to \infty$, as z then approaches the frictional isostaticity criterion $z = d+1$.

Contacts at the mobilization threshold slip with unchanged tangential forces if perturbed in the direction of mobilization. What are the consequences of this for

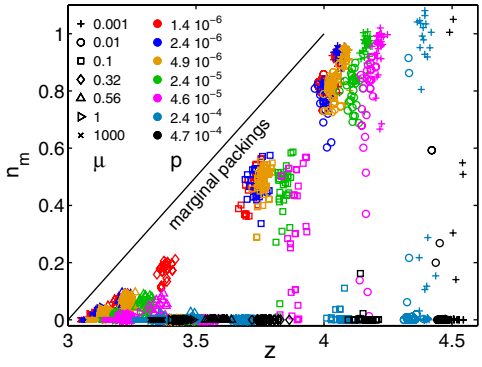

Fig. 1: (Color online) Position of our packing configurations in the phase space defined by z and n_m in our $2d$ simulations. The generalized isostaticity line $n_m = d(z - z^m_{\rm iso})/2 = z - 3$ is shown in black. Stable packings cannot exist to the left of this line. Each marker denotes one of 30 configurations at a given (μ, p) with the color-marker combinations indicated by the legend. For a given μ (a given symbol), configurations with larger p are to the right, and n_m drops to zero for the largest pressures.

the collective mechanical properties of frictional packings near jamming? In this letter, we show that the similarities between frictionless and frictional static sphere packings, which are brought to the foreground by this concept of generalized isostaticity, also extend to the dynamic properties. We do so by calculating the density of states (DOS) of frictional sphere packings, in the simplified limit where contacts with $m = 1$ slip in both directions with unchanged tangential forces during small amplitude vibrations.

We recover the low-frequency plateau in the DOS which is characteristic for packings of frictionless particles near jamming [2,3]. We find that the rescaled crossover frequency $\tilde{\omega}^* = \omega^*/p^{1/6}$ scales linearly with the distance from the generalized isostaticity line, as $\tilde{\omega}^* \sim (z - z^m_{\rm iso})$, see fig. 4. An analysis of the eigenmodes shows that the dominant low-energy displacements consist of particles rolling without sliding for contacts with $m \neq 1$, and tangential sliding at contacts with $m = 1$.

This scenario nicely generalizes the findings for frictionless spheres to the frictional case. Our findings stress the crucial role of the response of fully mobilized contacts. When instead of what we do here, these are all taken to be elastic, the inclusion of friction becomes a singular perturbation, and the excess low-frequency modes seen in frictionless packings are suppressed [6].

Simulation method. – We perform a numerical analysis of two-dimensional packings of frictional particles interacting with Hertz-Mindlin forces (during the preparation of the packings, energy is dissipated through viscous damping —see [5,6]). The Hertz-Mindlin interaction is comprised of a normal interaction that scales as $\delta^{3/2}$, where δ is the overlap of the particles, and an incremental tangential interaction which is limited by the Coulomb criterion $f_t \leqslant \mu f_n$ [19]. The packings are made at fixed friction coefficient μ and pressure p.

Motivated by eq. (1), we map the configurations in the phase space of fig. 1 spanned by z and n_m. The generalized isostaticity criterion $z = z^m_{\rm iso}$ then defines a *line of marginal packings* with end points $(z = 3, n_m = 0)$ and $(z = 4, n_m = 1)$, so that stable packings lie to the right of it. As in [5], we observe that for sufficiently gentle preparation methods, packings approach the generalized isostaticity line in the limit $p \to 0$.

The packing history is important here, since n_m is determined in the final stages of equilibration, when the packing structure, *i.e.* z, is already fixed. The system then follows a vertical path in the z-n_m phase diagram, and n_m reaches zero for insufficiently strong damping (see, *e.g.*, the configurations at $p = 4.6 \cdot 10^{-5}$ in fig. 1). For a system undergoing an avalanche, a similar variation of n_m fluctuating at fixed z was observed recently, with the largest n_m just before failure events [20]. There, failure was reached *before* reaching isostaticity, and linked to spatial correlations. We do not observe such correlations in the data presented here, though subtle effects could be responsible for the remaining gap between the generalized isostaticity line and the $p \to 0$ configurations. Hence we identify this line with the (zero pressure) jamming transition for slowly equilibrated frictional discs.

Treatment of small amplitude vibrations. – The vibrational density of states is obtained by linearizing the quations of motion around each stable state. Rattlers, which give rise to trival zero-frequency modes, are left out from the analysis from the start.

There are several subtleties associated with frictional response. The nature of the ideal Coulomb condition $|f_t| \leqslant \mu f_n$ implies a discontinous response for sliding displacements at fully mobilized contacts. For displacements which lead to an increase in the tangential force f_t (taking f_n fixed), the Coulomb condition implies that the contact slips with f_t unchanged. For displacements in the opposite direction, however, f_t *will* decrease proportional to the displacement. This then translates into a contact stiffness $k_t = 0$ in the slipping direction, but a finite k_t in the opposite direction!

This separation into two types of displacements at fully mobilized contacts is only meaningful for static-response studies, where the direction of perturbation remains fixed. Under vibrations, several effects come into play. Modes effectively couple through the Coulomb condition, since the total change of the force at a contact and hence n_m depends on all other modes present. Similarly, the displacements at different contacts of a particle are coupled, so that the mobilization at one contact will be influenced by its neighbors. Moreover fully mobilized contacts dissipate energy during the slipping half of the phase, and a decomposition into purely non-dissipative eigenmodes is not possible.

The situation is clearly complex, so we probe the importance of the fully mobilized contacts by considering two limiting cases. First, we simply put the tangential

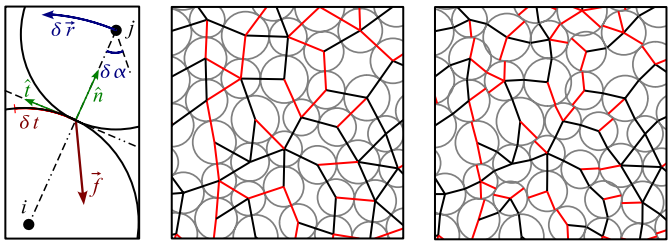

Fig. 2: (Color online) Left: contact geometry illustrating the various displacements and rotations as well as the effective tangential displacement δt of the contact point, where we have assumed that particle i is stationary. Middle and right: sample displacement for a low-energy eigenvector at $p = 1.41 \cdot 10^{-6}$ and $\mu = 0.001$. Middle: contact network in the initial state, with fully mobilized contacts in red. Right: particles have been displaced proportional to the mode amplitude. The lines now link the particle centers to the position of the *former* contact points. If $\delta t \neq 0$, the contact line between particles is broken.

stiffness $k_t = 0$ for all fully mobilized contacts: *fully mobilized contacts are treated as slipping contacts in both directions* which allows us to linearize the equations of motion and study the DOS of these modes. Then we compare this approach to the case where the fully mobilized contacts are treated elastically, and we establish the importance of the fully mobilized contacts through the fundamentally different results we obtain.

In light of the recent results for the avalanching system [20], we expect the first case to be relevant for systems where contacts are continuously driven towards full mobilization, for example by shear flow. Then $n_m > 0$ and sliding occurs at fully mobilized contacts, in the same direction as during the eventual failure. The second case is then relevant after failure events, when n_m has dropped. Sound vibrations form a marginal case, and therefore we compare both approaches here.

Within this framework, the equations of motion are conservative to first order, and their structure resembles what one finds for the vibrational properties of frictionless particles. After we expand the equation of motion around the equilibrium we obtain equations of motion of the form $\delta\ddot{r}_\alpha = -D_{\alpha\beta}\delta r_\beta + O(\delta r^2)$, where the dynamical matrix $D_{\alpha\beta}$ can, with the present simplifications and after a rescaling of the coordinates by the square root of the masses/moments of inertia, be written in terms of the derivatives of an effective potential, $D_{\alpha\beta} = (m_\alpha m_\beta)^{-1/2} \frac{\partial^2 V}{\partial \delta r_\alpha \delta r_\beta}$ [13]. For our packings with Hertz-Mindlin forces the effective potential is given by

$$V = \frac{1}{2}\sum_{\langle ij \rangle} \left[k_n (\vec{\delta r} \cdot \hat{n})^2 - \frac{f_n}{r^0} (\vec{\delta r} \cdot \hat{t})^2 + k_t \delta t^2 \right], \qquad (2)$$

where $\delta t = (\vec{\delta r} \cdot \hat{t}) - (R_i \delta\alpha_i + R_j \delta\alpha_j)$ is the tangential displacement of the contact point of the two particles, as illustrated in fig. 2. Here k_n and k_t are the normal and tangential stiffness, respectively, which derive from the Hertz-Mindlin interaction law and which both scale

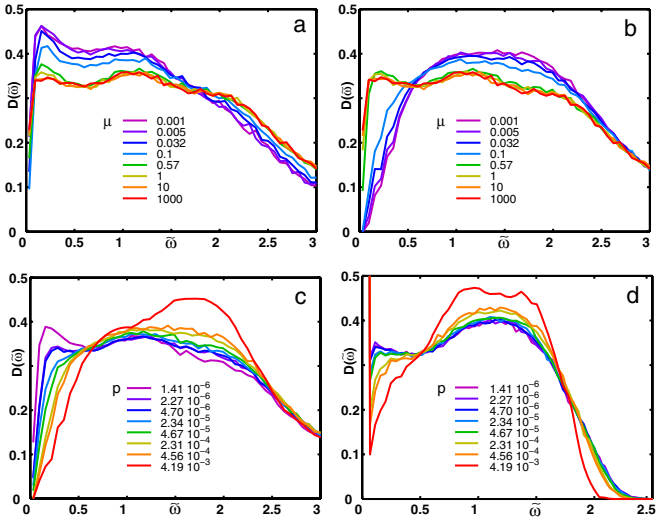

Fig. 3: (Color online) Density of states (DOS). (a) DOS with fully mobilized contacts treated as slipping for the smallest pressure $p = 1.41 \cdot 10^{-6}$ (approaching the line of generalized isostaticity) for a range of μ. (b) DOS for the same packings as in (a), but with all contacts treated as non-slipping, as in [6]. (c) Illustration of the low-frequency plateau developing in the DOS as p is decreased, for an intermediate friction coefficient $\mu = 0.3$ and with $m = 1$-contacts slipping. (d) DOS for range of pressures and $\mu = 0.001$, with the tangential stiffness constant set to $k_t^{1/2} = 10^{-3} k_n^{1/2}$ (see text).

as $k \sim \delta^{1/2}$ [19,21]. In this formulation, the vibrational spectrum is a histogram of the eigenvalues ω_k^2 of $D_{\alpha\beta}$ as a function of the associated frequencies ω_k.

Density of states. – We have studied the vibrational density of states (DOS) for a wide range of friction coefficients ($\mu \in [10^{-3}, 10^{3}]$) and pressures ($p \in [10^{-6}, 10^{-3}]$). We plot the density of states as a function of the rescaled frequencies $\tilde{\omega} = \omega / p^{1/6}$, appropriate for Hertz-Mindlin forces which exhibit a trivial softening with frequencies scaling as $\sqrt{k} \sim p^{1/6}$ [6].

Figures 3a, b show the DOS for the smallest pressure ($p = 1.41 \cdot 10^{-6}$), *i.e.*, close to the generalized isostaticity line, for the full range of μ. When the fully mobilized contacts are allowed to slip, the density of states clearly shows an excess number of low-energy modes (fig. 3a). Otherwise, when all contacts are chosen to have a finite k_t (no slipping contacts), the plateau in the DOS disappears for small friction coefficients, where n_m is large (fig. 3b and [6]).

In fig. 3c, we show the evolution of the density of states, again allowing fully mobilized contacts to slip, with increasing pressure for $\mu = 0.3$. The low-frequency part of the DOS shows linear $D(\tilde{\omega}) \sim \tilde{\omega}$ Debye-like behavior up to a normalized frequency $\tilde{\omega}^*$ which increases with pressure. In the frictionless case, $\tilde{\omega}^*$ scales as $z - z_{\rm iso}^0$ [2,3]. An extension of this argument then predicts for our frictional packings the scaling $\tilde{\omega}^* \sim z - z_{\rm iso}^m$ with in $2d$ the generalized isostatic contact number $z_{\rm iso}^m = 3 + n_m$ —we will verify this prediction below.

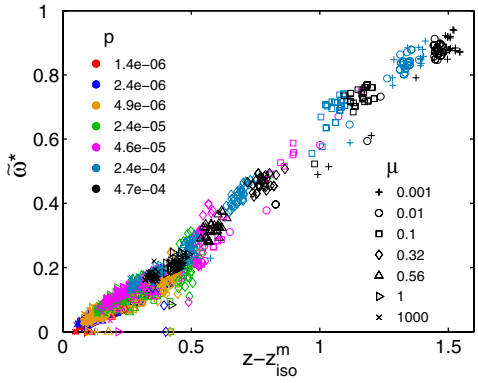

Fig. 4: (Color online) Normalized crossover frequency $\tilde{\omega}^*$ where the plateau in the DOS is reached as a function of the distance $z - (3 + n_m)$ from the line of generalized isostaticity. The relation is linear, in spite of the change of the μ-n_m relation at larger pressures (see fig. 1).

Even if the fully mobilized contacts are allowed to slip, the density of states for $\mu \to 0$ is still noticeably different from the frictionless case with $\mu = 0$ (although both have an excess of low-density modes). This is because the non-mobilized contacts still have a finite tangential stiffness k_t comparable to the stiffness for compression of bonds k_n, and hence a finite influence —this is even true when p approaches zero and the system approaches generalized isostaticity. Clearly, this non-smooth behavior has its root in the singular change of the dynamical matrix, due to the finite value of k_t of many contacts [6]. Figure 3d illustrates that when one takes the limit $k_t \to 0$ in the dynamical matrix, one recovers the frictionless DOS, with a peak of weight N due to trivial rotational modes at $\tilde{\omega} = 0$ [7]. We have checked that the width of the peak depends on the tangential stiffness constant, and our data supports the view that the peak will approach a δ-function when the tangential stiffness approaches zero.

Scaling of $\tilde{\omega}^*$. – To probe the scaling of the characteristic frequency with distance from the jamming point, we extract $\tilde{\omega}^*$ from the DOS. The characteristic frequency $\tilde{\omega}^*$ is determined by the point at which $D(\tilde{\omega})$ reaches a value of 0.2, normalized to the height of the plateau at $\tilde{\omega} = 1$, to avoid nonlinearities in the approach to the plateau. Figure 4 shows the $\tilde{\omega}^*$ we obtain for different μ and p as a function of $z - z_{\rm iso}^m$. The relation is linear to a good approximation, confirming our prediction.

Nature of the low-energy displacements. – We first determine the nature of the eigenmodes of the dynamical matrix in the $\tilde{\omega} \to 0$, $p \to 0$ limit from eq. (2). The prefactors of the tangential, normal and sliding displacements scale as $\delta^{3/2}$, $\delta^{1/2}$ and $\delta^{1/2}$, respectively, for a contact with $m \neq 1$. For a $m = 1$ contact, $k_t = 0$. Therefore, in the limit discussed above, the only low-energy displacement allowed for $m \neq 1$ is a purely tangential motion in combination with rotations of the particles in such a way that there is no tangential sliding. For $m = 1$ contacts, the movement

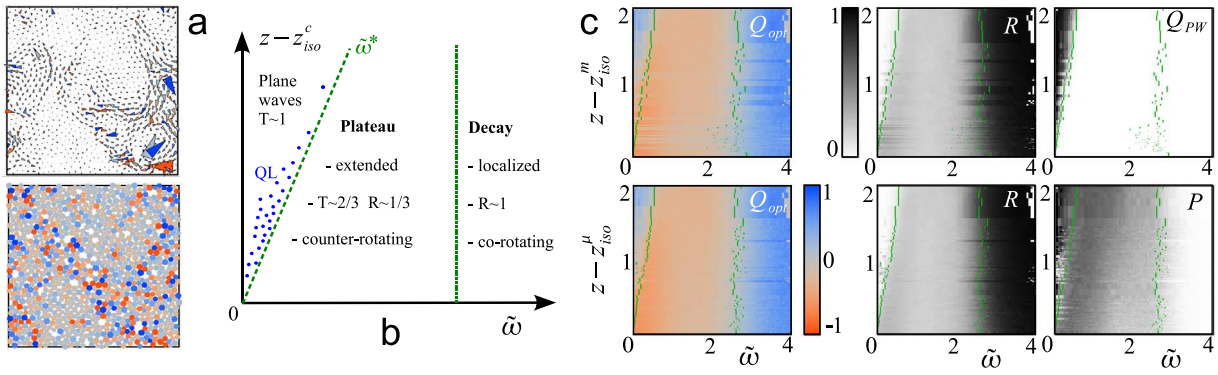

Fig. 5: (Color online) (a) Translational (top) and rotational (bottom) part of a low-energy ($\tilde{\omega}=0.1$) plateau eigenmode for a packing at $p=1.41\cdot10^{-6}$ and $\mu=0.1$. For the rotational part, the color scheme is red and blue for clockwise/counterclockwise rotations, and grayer shades for particles that rotate less. (b) Schematic phase diagram for the modes as a function of the distance from isostaticity. (c) Different order parameters characterizing the modes, with slipping contacts in the top row and non-slipping contacts in the bottom row. From left to right: optical rotation parameter $Q_{\rm opt}$ (see text), rotational energy fraction R, plane-wave fraction $Q_{\rm PW}$ (top, see text) and participation ratio P (bottom). The green lines are at $0.5\,\tilde{\omega}^*$ and the middle of the decay, respectively.

still has to be tangential, but sliding at the contact is permitted. A simple illustration of the displacements in a low-energy, low-p mode is shown in fig. 2: the difference in the rotational response between slipping fully mobilized contacts and non-slipping non-mobilized contacts is clearly visible.

The occurrence of floppy modes at generalized isostaticity, and the local rolling and sliding motion depending on the mobilization of the contact, can be understood from a counting argument. The $3N$ degrees of freedom of the packing participating in a floppy deformation need to satisfy two groups of constraints: setting the normal motion at each contact to zero gives $Nz/2$ constraints, while setting the sliding motion at each $m\neq1$ contact to zero gives $Nz/2-Nn_m$ constraints. Hence the number of constraints of the motion is exactly equal to the number of degrees of freedom only if $z=z^m_{\rm iso}=3+n_m$ —floppy modes arise at generalized isostaticity. Note that the variational argument of Wyart *et al.* [3] that estimates $\tilde{\omega}^*$ in terms of distorted floppy modes then generalizes in our case to $\tilde{\omega}^*\sim z-z^m_{\rm iso}$.

In the limit $\mu\to0$, we observe that $n_m\to1$ (every other contact is fully mobilized, see also [5]), so that at that point on the generalized isostaticity line, the $Nz/2-Nn_m=N$ contacts with $m\neq1$ equal precisely the number of rotational degrees of freedoms. Hence there are precisely enough contacts to couple the rotations to the translations. Unlike in the case of the spherical limit of ellipsoids, where the rotational modes appear in the gap of translational modes [7,8], here translations and rotations remain strongly coupled.

Structure of the modes. – We now characterize the full set of modes with relation to generalized isostaticity, and especially study the role of rotations. Our results, shown in fig. 5, confirm that for both slipping and non-slipping conditions, the distance to the respective isostatic value ($z^m_{\rm iso}$ or $z^\mu_{\rm iso}$) controls the properties of the packing.

We find three regimes. For $\omega<\omega^*$, the modes have a strong plane-wave component, which we estimate by the fraction $Q_{\rm PW}$ of the mode which is contained in the largest peaks of its Fourier transform $|\delta r_q|^2>50\langle|\delta r_q|^2\rangle$. We also determine the fraction of the vibrational energy that is stored in translational (T) and rotational (R) particle motion, and also find that these modes are almost purely translational, *i.e.* R is very small. Finally, using the participation ratio P [22–24], we find besides the extended plane waves a substantial fraction of modes with $P<0.1$ which are likely quasi-localized modes.

The second regime, which corresponds to the plateau in the DOS, is characterized by modes such as the one shown in fig. 5. They are extended, with a participation ratio $0.2\leqslant P\leqslant0.6$. Rotations contribute roughly 1/3 to the mode kinetic energy, while translations contribute 2/3. The rotations are "optical", *i.e.* neighboring particles tend to counter-rotate, while the translational lengthscales are much larger (see fig. 5). We quantify the counter-rotations through an optical order parameter $Q_{\rm opt}=\frac{\sum_{\langle ij\rangle}\delta\theta_i\delta\theta_j}{\sum_{\langle ij\rangle}\delta\theta_i^2}$, which is a type of phase quotient [25]. Clearly, the plateau is associated with negative values of $Q_{\rm opt}$.

The third regime corresponds to the decay of the DOS. These modes are almost purely rotational, with $R\to1$, and become progressively co-rotating with increasing ω so that $Q_{\rm opt}$ is positive (blue). As found in the frictionless case, these high-energy modes are localized with $P\to0$.

These results strongly resembles the frictionless case (see, *e.g.*, [23] for comparison), if we account for the different $z^c_{\rm iso}$ ($z^m_{\rm iso}$, $z^\mu_{\rm iso}$ and $z^0_{\rm iso}$ for the slipping, non-slipping and frictionless case, respectively).

Conclusion and outlook. – The jamming transition of frictional packing of spheres is more complex than the

transition at point J for frictionless spheres. However, we show that along the *generalized isostatic line* in the space spanned by the contact number z and the number of fully mobilized contacts n_m, the system shows critical behavior similar to the frictionless case if slipping contacts at $m = 1$ are incorporated into the dynamical matrix. In this case, the DOS shows a plateau near the $z^m_{\rm iso}$-line, and at larger pressure, the crossover frequency scales as $\tilde{\omega}^* \sim (z - z^m_{\rm iso})$.

While the physical relevance of treating fully mobilized contacts as freely slipping can be disputed, our study suggests that the precise details of the frictional interactions may have a profound effect on the linear response of frictional systems. In a more abstract sense, when we perceive our system as strictly composed of a mix of slipping and frictional contacts, our investigation also successfully tests that the relation between ω^* and constraint counting arguments remains valid for situations more complicated than purely frictionless spheres.

Our works suggests various topics for further investigations. First, the relation between the friction coefficient and n_m is poorly understood except for the limiting cases $\mu \to \infty$ and $\mu \to 0$. Our simulations indicate that this relation depends significantly on the preparation method of the sample, where packings prepared with higher viscous damping have larger n_m [13].

Second, the z-n_m phase diagram can be a tool to understand the behavior of more complex dynamics. Simulations evidence that a substantial part of the movement of frictional piles is due to contacts failing at the mobilization threshold [10,14,16,20,26,27]. As mentioned above, for a sheared packing, the number of fully mobilized contacts increases until a rearrangement occurs, then it drops. The system can build up mobilization again by applying further shear. Similarly, in a system undergoing an avalanche, the number of fully mobilized contacts increases before the system fails, so that the system moves along a vertical path in the z-n_m space [16,20].

Third, nonlinearities and dissipation at the contact must have a strong effect for finite perturbations. For example, it can be shown that applying a finite sinusoidal perturbation to a fully mobilized contact destroys this contact in the presence of dissipation. On the other hand, repeated shear can regenerate fully mobilized contacts. We plan to use molecular-dynamics simulations to investigate the response of the system beyond linear order, and to have a clearer understanding of the importance of fully mobilized contacts within the framework of the z-n_m phase diagram.

* * *

We are grateful to K. Shundyak for help and use of his packings. SH gratefully acknowledges support from the physics foundation FOM.

REFERENCES

[1] O'Hern C. S., Silbert L. E., Liu A. J. and Nagel S. R., *Phys. Rev. E*, **68** (2003) 011306.
[2] Silbert L. E., Liu A. J. and Nagel S. R., *Phys. Rev. Lett.*, **95** (2005) 098301.
[3] Wyart M., Silbert L. E., Nagel S. R. and Witten T. A., *Phys. Rev. E*, **72** (2005) 051306.
[4] Ellenbroek W. G., Somfai E., van Hecke M. and van Saarloos W., *Phys. Rev. Lett.*, **97** (2006) 258001.
[5] Shundyak K., van Hecke M. and van Saarloos W., *Phys. Rev. E*, **75** (2007) 010301 (R).
[6] Somfai E., van Hecke M., Ellenbroek W. G., Shundyak K. and van Saarloos W., *Phys. Rev. E*, **75** (2007) 020301 (R).
[7] Zeravcic Z., Xu N., Liu A. J., Nagel S. R. and van Saarloos W., *EPL*, **87** (2009) 26001.
[8] Mailman M., Schreck C. F., O'Hern C. S. and Chakraborty B., *Phys. Rev. Lett*, **102** (2009) 255501.
[9] Majmudar T. S. and Behringer R. P., *Nature*, **435** (2005) 1079.
[10] Antony S. J. and Kruyt N. P., *Phys. Rev. E*, **79** (2009) 031308.
[11] Anthony J. L. and Marone C., *J. Geophys. Res.*, **110** (2005).
[12] Zhang H. P. and Makse H. A., *Phys. Rev. E*, **72** (2005) 011301.
[13] Henkes S., Shundyak K., van Hecke M. and van Saarloos W., in preparation.
[14] Silbert L. E., Ertaş D., Grest G. S., Halsey T. C. and Levine D., *Phys. Rev. E*, **65** (2002) 051307.
[15] Bouchaud J.-P., *Proceedings of Les Houches Session LXXVII*, edited by Barrat J.-L., Feigelman M., Kurchan J. and Dalibard J. (Springer, Heidelberg) 2004.
[16] Deboeuf S., Dauchot O., Staron L., Mangeney A. and Vilotte J.-P., *Phys. Rev. E*, **72** (2005) 051305.
[17] Unger T., Kertész J. and Wolf D. E., *Phys. Rev. Lett.*, **94** (2005) 178001.
[18] Song C., Wang P. and Makse H. A., *Nature*, **453** (2008) 629.
[19] Johnson K. L., *Contact Mechanics* (Cambridge University Press) 1985.
[20] Henkes S., Brito C., Dauchot O. and van Saarloos W., arXiv:1001.2202v1 (2010).
[21] Somfai E., Roux J.-N., Snoeijer J. H., van Hecke M. and van Saarloos W., *Phys. Rev. E*, **72** (2005) 021301.
[22] Zeravcic Z., van Saarloos W. and Nelson D. R., *EPL*, **83** (2008).
[23] Silbert L. E., Liu A. J. and Nagel S. R., *Phys. Rev. E*, **79** (2009) 021308.
[24] Xu N., Vitelli V., Liu A. J. and Nagel S. R., arXiv:0909.3701v1 (2009).
[25] Bell R. J. and Hibbins-Butler D. C., *J. Phys. C: Solid State Phys.*, **8** (1975).
[26] Wyart M., *EPL*, **85** (2009) 24003.
[27] Landry J. W. and Grest G. S., *Phys. Rev. E*, **69** (2004) 031303.